RSC Advances

Journal Name

ARTICLE TYPE

Effect of Ligands on Characteristics of $(CdSe)_{13}$ Quantum Dot

Yang Gao, [Δ,a] Bo Zhou, [Δ,b] Seung-gu Kang, [c] Minsi Xin, [a] Ping Yang, [d] Xing Dai, [a] Zhigang Wang*, [a,e] and Ruhong Zhou*, [a,c,f]

5

The widespread applications of quantum dots (QDs) have spurred an increasing interest in the study of their coating ligands, which can not only protect the electronic structures of the central QDs, but also
10 control their permeability through biological membranes with both size and shape. In this work, we have used density functional theory (DFT) to systematically investigate the electronic structures of $(CdSe)_{13}$ passivated by $OPMe_2(CH_2)_nMe$ ligands with different lengths and various numbers of branches (Me=methyl group, n = 0, 1-3) as well as different number of ligands $((CdSe)_{13}+[OPMe_2(CH_2)_2Me]_m$ (m = 0, 1, 9, 10)). Our results show that the absorption peak in the ultraviolet-visible (UV-vis) spectra
15 displays a clear blue-shift, on the scale of ~100 nm, upon the binding of ligands. Once the total number of ligands bound with $(CdSe)_{13}$ reached a saturated number (9 or 10), no more blue-shift occurred in the absorption peak in the UV-vis spectra. On the other hand, the aliphatic chain length of ligands has a negligible effect on the optical properties of the QD core. Analyses of the bonding characteristics confirm that optical transitions are dominantly governed by the central QD core rather than the organic
20 passivation. These findings might provide insights on the material design for the passivation of quantum dots for biomedical applications.

Introduction

The unique optical properties of quantum dots (QDs) have been widely applied to the design of functional materials, including
25 photoenergy converters and nano-sized sensors[1-9]. Their versatilities are largely originated from QDs' easy adaptability on various physicochemical factors such as particle sizes, atomic compositions, and surface modifications[10-17]. More interestingly, inorganic QDs with comparable sizes to many biomolecules are
30 recently proposed as potential platform for nanodrug carriers and/or diagnostic agents[18-29]. These advances have raised serious requirements on a solid premise on the biosafety of QDs in a highly degradable biological environment.

Biocompatibility is usually achieved by the surface passivation
35 on QDs with biocompatible organic molecules, so as to secure the toxic QDs in the core as well as to avoid their direct contacts with biomolecules[26, 30]. The passivation is also inevitable in stabilizing and dispersing QDs in an aggregation-prone aqueous medium, where the organic layer reduces the highly reactive surface
40 potential[31-33], an intrinsic property of colloidal semiconductor

nanoparticles due to high curvature[20, 21]. As such, the surface modification is accompanied by its critical influence to the chemical and electronic structures of QDs[11, 16]. Recent theoretical studies show that the passivating ligands can form stable
45 coordinations on QD surface, sustaining the chemical structure of the QD[31-34]. On the other hand, experimental study (e.g. PbSe QD) revealed a complex behaviour between the PbSe-QD core and passivating organic layer in controlling the optical property[35]. Thus, it is crucial to understand electrochemical effect of the
50 passivating ligands on QDs in developing biocompatible and stable QDs, while simultaneously maintaining their desired electro-optical functions [36].
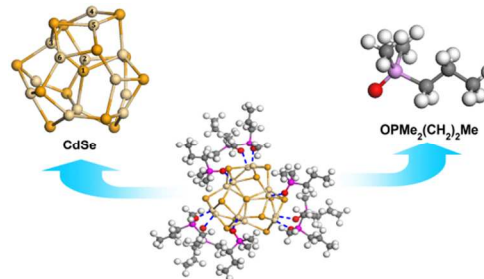

Fig. 1 Left: The optimized bare $(CdSe)_{13}$-cage structure with C_3

symmetry ; Right: a single ligand structure: $OPMe_2(CH_2)_2Me$; Middle: the optimized $(CdSe)_{13}+9OPMe_2(CH_2)_2Me$ complex structure with C_3 symmetry. The dotted lines indicate the ligand passivated sites. (Cd: faint yellow, Se: deep yellow, O: red, P: pink, C: gray, and H: white. similarly hereinafter)

Here, we systematically investigate the ligand effect on the electronic structure of a typical $(CdSe)_{13}$ quantum dot[37-39]. A bare CdSe-QD is toxic which can cause massive cell deaths in vivo tests[26, 30], despite its excellent optical property and promising potential for biomedical applications. Thus, an effective passivation would be a critical step for avoiding any detrimental effect on the host biosystem as well as stabilizing the chemical and structural integrity of the QD[40, 41]. A spherical structure of $(CdSe)_{13}$ and a large surface-to-volume ratio facilitate a high density coating with various organic ligands[25-28]. Among many available ligands coupled to CdSe-QDs[42-47], we selected trimethyl phosphine oxide (TMPO) and its derivatives (i.e,. $OPMe_2(CH_2)_nMe$, n=0, 1-3) due to their high ligand exchange capacity on the CdSe surface[48]. Despite several studies on this important ligand coating[17, 34, 48], there are still quite a few interesting questions remaining, such as what kind of length effect the ligand might have, whether the number of branches matter, and how sensitive the coating is to the number of ligands. In this study, we used the first-principal density functional theory (DFT) to systematically study these important effects, which has been proven as a useful methodology for similar systems of molecular adsorption[17, 31-33, 42-52]. We investigated the optical property changes of the $(CdSe)_{13}$ core, including electronic spectra, electron transfer and density of state, binding energy with varying surface capping density and alkyl chain length of the passivation ligands.

Computational Methods

The structure of the bare $(CdSe)_{13}$ QD was revealed from mass spectrometry, which could exist as a stable cage structure[37]. Cadmium ions were determined as the primary cause of cytotoxicity in their applications in vivo[30]. The passivated structures have thus been generated with TMPO on top of the toxic Cd atoms[30]. In order to study the capping density effect, we prepared three different systems depending on numbers of TMPOs (i.e., 1, 9 and 10; Supporting Information Part 1). The ligands were firstly set to coordinate the unsaturated Cd atoms for cases of 1 and 9 TMPOs. The last ligand with 10 TMPOs was placed on the saturated Cd atom (i.e., Cd (2) in Fig 1), which was

located on the axis of the 3-fold symmetry of the $(CdSe)_{13}$-cage. For the effect of alkyl chain lengths of the passivated ligands, we also varied the chain length of one of the methyl groups of TMPO from methyl to butyl (i.e., $OPMe_2$-$(CH_2)_nMe$, n = 0, 1-3).

Previous study have shown that the hybrid exchange correlation functional B3LYP[53-55] of DFT with LANL2DZ basis set is appropriate for describing electronic properties of CdSe QDs, Whether it is pure theory or the combination of the theoretical and experimental work[48, 52, 56-60]. And the organic passivation undergoes with a weakly-coupled interaction which is based on electrostatic interaction formation[34], rather than the weak van der Waals interaction between molecules. Thus the results of the DFT-B3LYP method without the empirical dispersion term have been gived in the text, and a compare with the results including the empirical dispersion contribution (using the B3LYP-D3 method) was performed in the Supporting Information part 2. Accordingly, the B3LYP method was employed to optimize all geometric structures[17]. Considering that the molecular passivation may create atypical bonds, we added d polarization functions for all the C, O, and P atoms, and also added p polarization functions for all the H atoms by using double-ξ basis set [61] for the ligands. We also examined the symmetry effect on the molecular geometry and electronic structures by imposing the systems with C_3 symmetry[37]. The vibrational frequencies were calculated at the same level of theory to verify the minima of the corresponding structures (Supporting Information part 3). In addition, the time-dependent density functional theory[62] (TD-DFT) was also used to study UV-vis absorption spectra. Previous research has shown the solvent effect is not significant on UV-vis spectra of passivated CdSe QD system[33]，therefore it will not be introduced in the calculation. All the calculations were performed with the Gaussian 09 program package[63].

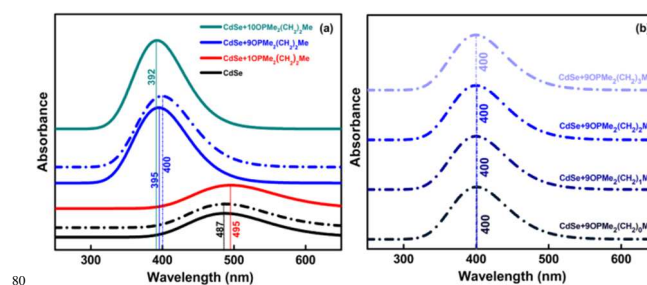## RESULTS and DISCUSSION

UV-vis absorption spectra of QD

Fig. 2 The UV-vis absorption spectra of $(CdSe)_{13}$+$[OPMe_2$-

(CH₂)₂Me]ₘ (m = 0, 1, 9, 10). Different colors represent different QD complex structures. Dash-dot lines represent the corresponding structure with C_3 symmetry. The numbers indicate the wavelengths of electronic absorption peaks.

5

It is well established that CdSe-QD has unique optical properties. In this work, we first focus on the significant absorption peak with the maximum excitation wavelength, which is contribution by valence orbital transitions, and the calculated
10 results is comparable with previous reports (Supporting Information part 4).The UV-vis absorption spectra are dramatically shifted upon passivation, where the peak is blue-shifted by ~95 nm from 487 nm of the bare QD core (Fig 2a). However, it seems converged to ~395 nm after 9 ligands,
15 whereafter the peak moves only 3 nm to the blue (i.e., 392 nm) with 10 ligands. On the contrary, the UV-vis spectra are not sensitive to the allipatic chain length of the coordinated ligands (Fig 2b). Our result clearly indicates that the organic passivation has a significant effect on electronic absorption bands of the
20 CdSe core. Similar blue-shift effect is consistent with recent study on UV-vis spectra of $(CdSe)_{13}$ passivated by methylamine ligands[56]. And then, we also considered the effect of dispersion

45

interaction between QD and ligands on the UV-vis spectra using the B3LYP-D3 method and found that the max absorption peak
25 has only a little blue-shift (about 10 nm) compared with the result above (Supporting Information Part 2).

In order to further validate our current theoretical approach, we compared our findings with available data from previous studies. There are several previous studies with both theoretical
30 and experimental methods on the UV-vis spectra of CdSe QDs[64-66]. Table S1 (Supporting Information Part 4) summarizes UV-vis spectra observed for various sizes of QDs saturated in TOPO solvent. It is clear that the maximum excitation wavelength decreases from 550 nm to 415 nm as with decrease of particle
35 size 3.1 nm to 1.2 nm. Since the experimental results are all for QD nanostructures of larger than our system of ~0.9 nm, it is difficult to directly compare[67]. Nonetheless, the trend seems reasonable to be extrapolated to our calculated excitation wavelength 400 nm. In other words, with the decrease of the size
40 of the center quantum particles, the excitation wavelength displays a clear blue-shift. In this work, the diameter of the bare $(CdSe)_{13}$-cage is 0.9 nm, so it can be inferred from Table S1 that the maximum excitation wavelength should be less than 415 nm, which agrees well with our result of about 400 nm.
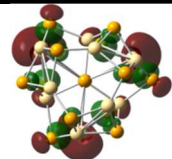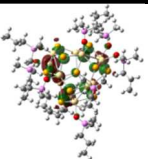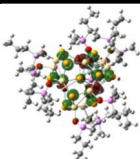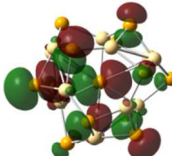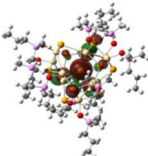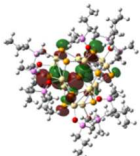
Table 1 The excitation energies (E in eV), excitation wavelength (λ in nm), oscillator strengths (f>0), and excited-state composition with contribution percentages [similar statistical methods have been reported [68-70]] of the two kinds of asymmetrical structure.

structure	E	λ	f	Transition
$(CdSe)_{13}$	2.52	493	0.032	49% HOMO-2 [Cd 5p 5%, Se 4p 95%] →LUMO [Cd 5s 70%, Se 4p 30%]
	2.56	485	0.030	1% HOMO-1 [Cd 5p 8%, Se 4p 92%] →LUMO
				47% HOMO [Cd 5p 8%, Se 4p 92%] →LUMO
	2.56	485	0.030	47% HOMO-1→LUMO
				1% HOMO→LUMO
$(CdSe)_{13}+9OPMe_2(CH_2)_2Me$	3.02	411	0.085	49% HOMO [Cd 5p 6%, Se 4p 94%] →LUMO [Cd 5s 68%, Se 4p 32%]
	3.13	396	0.096	48% HOMO-1 [Cd 5p 7%, Se 4p 93%] →LUMO
	3.23	384	0.125	2% HOMO-3 [Cd 5p 9%, Se 4p 91%] →LUMO
				46% HOMO-2 [Cd 5p 8%, Se 4p 92%] →LUMO

On the other hand, Table S2 (Supporting Information Part 4) shows the peak positions of the 0.9 nm $(CdSe)_{13}$-cage depending on degree of passivation. They ranges from 487 nm in bare

5 $(CdSe)_{13}$ to 400 nm in $(CdSe)_{13}+9OPMe_2(CH_2)_{0, 1-3}$Me-symmetry passivation. As shown above, passivation obviously induced significant blue-shift in the excitation wavelength, consistent with previous findings[71]. These comparisons confirmed that our current approach is reliable.

10 We then computed the detailed excitation transition energies, oscillator strengths, and related molecular orbital composition, to further understand the origin of the electronic absorption peak (Table 1 and Supporting Information Part 5). Electronic transitions mostly occurred in four highly occupied

15 molecular orbitals (i.e., HOMO-3 to HOMO). For example, $(CdSe)_{13}+9OPMe_2(CH_2)_2$Me shows the electronic transition from the first four front occupied orbitals to LUMO, where the symmetry constraint only causes a few nanometer shift of the absorption peaks. It is noteworthy that all the electronic

20 transitions are only originated from the central QDs, independent of ligands. The orbital localization is depicted in Table 2 and S4 (Supporting Information Part 6), where HOMO and LUMO are dominantly created in the CdSe-core regardless of the ligands. The vibration spectra clearly show that there is no collaborative

25 vibration between central $(CdSe)_{13}$ and ligands (Supporting Information Part 2).

Table 2 The highest occupied molecular orbital (HOMO) and the lowest unoccupied molecular orbital (LUMO) of bare $(CdSe)_{13}$ cage

30 asymmetrical structure, $(CdSe)_{13}+9OPMe_2(CH_2)_2$Me asymmetrical structure and $(CdSe)_{13}+10OPMe_2(CH_2)_2$Me structure.

MO	$(CdSe)_{13}$	$(CdSe)_{13}+$ $9OPMe_2(CH_2)_2$Me	$(CdSe)_{13}+$ $10OPMe_2(CH_2)_2$Me
LUMO			
HOMO			

Mulliken charge populations for CdSe

In addition, the charge delocalization can be assessed by the

35 extent of charge transfer, which is found to be relatively small overall. Using the case of $(CdSe)_{13}+9OPMe_2(CH_2)_n$Me (n=0, 1-3) as an example, Mulliken charge populations are varied by less than 0.1 e for the representative core atoms (i.e., Se(1), Cd(2), Cd(4), Cd(5), Cd(6)) from the various passivation. Also,

40 compared to the bare system ($Cd_{13}Se_{13}$), QDs with surface passivation are slightly easier to lose and obtain electrons for Cd and Se atoms, respectively. Nevertheless, the net charge transfer in $(CdSe)_{13}+9OPMe_2(CH_2)_3$Me (from the ligands to the core) is only about 0.156 e per ligand.
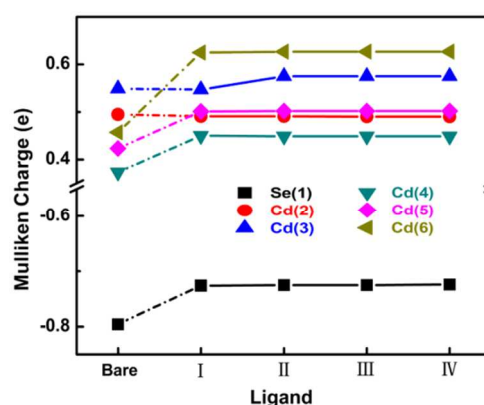
45

Fig. 3 Mulliken partial charge populations for surface Se and Cd atoms. The positions of these atoms are shown in Fig 1(left) in which the numbers are corresponding to the position of Se and Cd. The

50 abscissa I, II, III, and IV represents bare $(CdSe)_{13}$-cage symmetrical structures and $(CdSe)_{13}+9OPMe_2(CH_2)_n$Me (n=0, 1-3) symmetrical structures, respectively.

The chain length has a negligible effect on the charge

55 distribution, which is particularly obvious for atoms Cd(2) and Cd(3) due to no dangling bonds for passivating ligands. It is also non-sensitive with the symmetry constraint (see red and blue curves in Fig 3). This indicates that there is no obvious chemical bonding between QD and ligands (Supporting Information Part 7),

60 but only partial charge polarization. Our results support that the CdSe-QD is kept stable even with TMPO saturated on the surface, which would be important for QD to properly serve as an optical probe in the highly degradable biological media, although the optical properties are tuned by the degree of passivation.

65

DOSs of the system

We calculated the density of states (DOSs) of the system. The DOS varies sensitively depending on the degree of passivation (Fig 4a). The Fermi level is shifted up to ~2.5 eV. The HOMO-LUMO gap increased from 3.0 eV to 3.6 eV for the bare and the passivated systems (Supporting Information Part 4), respectively, further confirming the significant blue-shifts in aforementioned UV-vis spectra. This is also qualitatively consistent with recent experiment with $(CdSe)_6$ passivated by OPH_3[52]. Especially, DOS are highly fluctuating between -10.0 and -16.0 eV with the increase of passivation. These fluctuations are mainly contributed by ligands. From orbital component analysis we found that these ligand molecular orbitals (MOs) are mostly localized on the 2p orbitals of C atoms, 2p orbitals of O atoms, and 3p orbitals of P atoms. On the other hand, the fluctuations in DOS from -6.5 and -10 eV are from MOs of Se and Cd atoms, which are strongly localized on the 4p orbitals and 5s orbitals for Se and Cd respectively. There are also some hybrid orbitals between QD and ligands. DOSs becomes stable once ligands are saturated (after nine ligands). On the contrary, DOSs are relatively less sensitive to the symmetry constraints and the chain length variation (Fig 4b). The shift is only about 10^{-2} eV for Fermi levels of QDs with different chain lengths. Interestingly, the density of states (DOS) share similar characteristics as vibrational spectra (Supporting Information Part 3), even though there is no coordination vibration mode between the ligands and the central QD. Therefore, we conclude that the increase of the chain length of ligands would not significantly affect the energy level position of the QD.
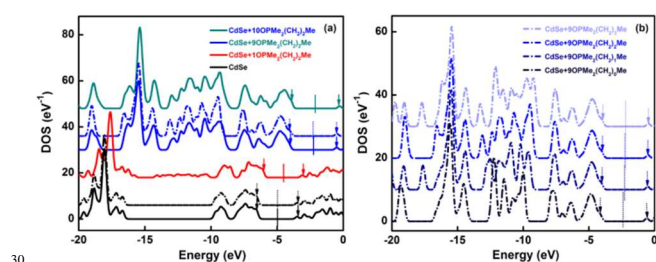

Fig. 4 The different QD structures of DOSs. The dash-dot and solid lines represent symmetry and asymmetry, respectively. The arrows represent the position of HOMOs and LUMOs in different structures and the vertical dotted lines indicate the Fermi level.

The stability of the ligand coating on the $(CdSe)_{13}$ surface is further studied. We calculated the average binding energy E_b per each ligand molecule between the ligand and the $(CdSe)_{13}$ cluster. E_b is defined as

$$E_b = \frac{1}{n}[E_{(CdSe)13+Ligands} - (E_{relaxed}^{(CdSe)13} + E_{relaxed}^{Ligands})]$$

where $E_{(CdSe)13+Ligands}$ is the total energy of the ligands coating on the $(CdSe)_{13}$ surface, while $E_{relaxed}^{(CdSe)13}$ and $E_{relaxed}^{Ligands}$ represent the total energies of $(CdSe)_{13}$ and ligands in its relaxed geometry, respectively, with both the $(CdSe)_{13}$ and ligands being in the same atomic configurations as in the relaxed $(CdSe)_{13}$+ligands system.

Our calculations show the binding energy E_b is -1.15 eV for each $OPMe_2(CH_2)_2Me$ when absorbing onto the $(CdSe)_{13}$ surface, which is comparable to a recent theoretical study, -1.08 eV/ligand for $(CdSe)_6$ passivated by $OPMe_3$[57]. We also calculated the average binding energy E_b for $(CdSe)_{13}$+ $9OPMe_2(CH_2)_nMe$ (n=0, 1-3) structures, and the resulting binding energies are 0.88 eV, 0.89 eV, 0.89 eV and 0.89 eV respectively for n=0, 1-3 (Supporting Information Part 8), which suggests the chain length has only minor effect on the binding energy, consistent with above electronic structure analyses. These binding energies also suggest the $(CdSe)_{13}$ clusters passivated by various $OPMe_2(CH_2)_nMe$ ligands are quite stable. Furthermore, the IR vibrational spectra data also support that the QD is stable with only relatively weak coupling to the passivation organic molecules (Supporting Information part 3).

Conclusions

In this work, we systematically studied the electronic structures of $(CdSe)_{13}$ nanocluster passivated TMPO ligands, with different chain lengths, different number of branches, and different number of ligands. Our calculations indicate that the coating ligands can significantly blue-shift the position of the absorption peaks of UV-vis spectra (on the scale of 95 nm). Once the passivation is saturated on the surface of $(CdSe)_{13}$ (i.e., 9 ligands in this case), the absorption peaks in the UV-vis spectra tend to be stabilized. The analyses of valence MOs of passivated QD structures indicate that the active orbital regions are localized in the center of $(CdSe)_{13}$ QD. Moreover, from the UV-vis spectra of $(CdSe)_{13}$ coated with 9-ligands, we find that $(CdSe)_{13}$ QD is insensitive to the branch length of ligands. Similar conclusion is also reflected in the binding energy, DOS spectra and vibration spectra.

Since CdSe QDs are widely used in many applications including biomedical ones, it is critical to fully understand their

electronic structures as well as effects from coating ligands. Our current extensive study clearly shows that the optical characteristics of QD will not change much even in the saturated passivation as well as the length variation of ligand aliphatic chains. Even though our current findings are based on $(CdSe)_{13}$, we believe these conclusions can be applied to other QDs of different sizes, and provide new insight on biomedical applications of QDs.

Acknowledgments

Notes and references

[a]Institute of Atomic and Molecular Physics, Jilin University, Changchun, 130012, China

[b]Bio-X Lab, Department of Physics, Zhejiang University, Hangzhou, 310027, China

[c]Computational Biology Center, IBM Thomas J. Watson Research Center, Yorktown Heights, NY 10598

[d]Environmental Molecular Sciences Laboratory, Pacific Northwest National Laboratory, Richland, WA 99352

[e]State Key Laboratory of Theoretical and Computational Chemistry, Institute of Theoretical Chemistry Jilin University, Changchun, 130023, China

[f]Department of Chemistry, Columbia University, New York, NY 10027

[Δ]*These authors contributed equally to this work.*

E-mail: wangzg@jlu.edu.cn; ruhongz@us.ibm.com

† Electronic Supplementary Information (ESI) available: [The bare $(CdSe)_{13}$-cage structure. The dispersion correction of UV UV-vis absorption spectra. The vibration modes of central QD and the vibration spectra with different number/length of ligands. Comparison of our calculated results with previous reports. The excitation energy, oscillator strengths and corresponding molecular orbital compositions of QDs. Molecular valence orbitals of $(CdSe)_{13}$ with ligands. Contour maps of charge density deformation in the local area of Cd and O atoms. The average binding energy E_b for per ligand molecule between the ligands and the $(CdSe)_{13}$ clusters. References for the Supporting Information]. See DOI: 10.1039/b000000x/

1. M. Bruchez, M. Moronne, P. Gin, S. Weiss, A. P. Alivisatos, *Science.* 1998, **281**, 2013–2016.

2. N. Tessler, V. Medvedev, M. Kazes, S. Kan, U. Banin, *Science.* 2002, **295**, 1506–1508.

3. J. Gorman, D. G. Hasko, D. A. Williams, *Phys. Rev. Lett.* 2005, **95**, 090502.

4. S. Csonka, I. Weymann, G. Zarand, *Nanoscale*, 2012, **4**, 3635-3639.

5. J. Y. Lek, L. Xi, B. E. Kardynal, L. H. Wong, Y. M. Lam, *ACS Appl. Mater. Interfaces.* 2011, **3**, 287-292.

6. P. V. Kamat, *J. Phys. Chem. C.* 2008, **112**, 18737–18753.

7. I. Lokteva, N. Radychev, F. Witt, H. Borchert, J. Parisi, J. Kolny-Olesiak, J. Phys. Chem. C. 2010, 114, 12784–12791.

8. D. Gerion, F. Pinaud, S. C. Williams, W. J. Parak, D. Zanchet, S. Weiss, A. P. Alivisatos, *J. Phys. Chem. B.* 2001, **105**, 8861–8871.

9. D. A. Tryk, A. Fujishima, K. Honda, *Electrochimica. Acta.* 2000, **45**, 2363–2376.

10. A. P. Alivisatos, *Science.* 1996, **271**, 933–937.

11. A. Pandey, P. Guyot-Sionnest, *Science.* 2008, **322**, 929–932.

12. C. B. Murray, D. J. Norris, M. G. Bawendi, *J. Am. Chem. Soc.* 1993, **115**, 8706–8715.

13. A. Shiohara, S. Prabakar, A. Faramus, C. Y. Hsu, P. S. Lai, P. T. Northcote, R. D. Tilley, *Nanoscale*, 2011, **3**, 3364-3370.

14. L. H. Qu, X. G. Peng, *J. Am. Chem. Soc.* 2002, **124**, 2049–2055.

15. G. D. Scholes, G. Rumbles, *Nat. Mater.* 2006, **5**, 683–696.

16. M. Beard, A. Midgett, M. Law, R. Ellingson, A. Nozik, *Nano. Lett.* 2009, **9**, 1217–1222.

17. S. Kilina, S. Ivanov, S. Tretiak, *J. Am. Chem. Soc.* 2009, **131**, 7717–7726.

18. S. G. Kang, G. Q. Zhou, P. Yang, Y. Liu, B. Y. Sun, T. Huynh, H. Meng, L. Zhao, G. M. Xing, C. Y. Chen, Y. L. Zhao, R. H. Zhou, *PNAS.* 2012, **109**. 15431–15436.

19. S. G. Kang, T. Huynh, R. H. Zhou, *Sci. Rep.* 2012, **2**, 00957.

20. W. J. Parak, D. Gerion, T. Pellegrino, D. Zanchet, C. Micheel, S. C. Williams, R. Boudreau, M. A. L. Gros, C. A. Larabell, A. P. Alivisatos, *Nanotechnology.* 2003, **14**, R15–R27.

21. X. Michalet, F. Pinaud, T. D. Lacoste, M. Dahan, M. P. Bruchez, A. P. Alivi-satos, S. Weiss, *Single Mol.* 2001, **2**, 261–276.

22. X. Michalet, F. F. Pinaud, L. A. Bentolila, J. M. Tsay, S. Doose, J. J. Li, G. Sun-daresan, A. M. Wu, S. S. Gambhir, S. Weiss, *Science.* 2005, **307**, 538–544.

23. I. L. Medintz, H. T. Uyeda, E. R. Goldman, H. Mattoussi, *Nat. Mater.* 2005, **4**, 435–446.

24. R. Gill, M. Zayats, I. Willner, *Angew. Chem. Int. Ed.* 2008, **47**, 7602–7625.

25. C. S. S. R. Kumar, Nanomaterials for Medical Applications. Kirk-Othmer Encyclopedia of Chemical Technology, Wiley, 2007. http://mrw.interscience.wiley.com/emrw/9780471238966/kirk/article/nanokuma.a01/current/abstract. Accessed February 11, 2008.

26. J. Drbohlavova, V. Adam, R. Kizek, J. Hubalek, *J. Mol. Sci.* 2009, **10**, 656-673.

27. M. S. Andrew, S. M. Nie, *Nat. Biotechnol.* 2009, **27**, 732–733.

28. M. S. Andrew, S. M. Nie, *J. Am. Chem. Soc.* 2008, **130**, 11278–11279.

29. Y. Wang, Y. H. Liu, Y. Zhang, F. Wang, P. J. Kowalski, H. W. Rohrs, R. A. Loomis, M. L. Gross, W. E. Buhro, *Angew. Chem., Int. Ed.* 2012, **51**, 6154–6157.

30. M. A. Walling, J. A. Novak, J. R. E. Shepard, *J. Mol. Sci.* 2009, **10**, 441-491.

31. S. Y. Chung, S. Lee, C. Liu, D. Neuhauser, *J. Phys. Chem. B.* 2009, **113**, 292-301.

32. H. Kim, S. W. Jang, S. Y. Chung, S. Lee, *J. Phys. Chem. B.* 2010, **114**, 471–479.

33. V. V. Albert, S. A. Ivanov, S. Tretiak, S. V. Kilina, *J. Phys. Chem. C.* 2011, **115**, 15793–15800.

34. J. M. Azpiroz, J. M. Matxain, I. Infante, X. Lopez, J. M. Ugalde, *Phys. Chem. Chem. Phys.* 2013, **15**, 10996-1005.

35. C. M. Evans, L. Guo, J. J. Peterson, Z. S. Maccagnano, T. D. Krauss, *Nano. Lett.* 2008, **8**, 2896−2899.

36. A. Nag, A. Hazarika, K. V. Shanavas, S. M. Sharma, I. Dasgupta, D. D. Sarma, *J. Phys. Chem. Lett.* 2011, **2**, 706−712.

37. A. Kasuya, R. Sivamohan, Yu. A. Barnakov, I. M. Dmitruk, T. Nirasawa, V. R. Romanyuk, V. Kumar, S. V. Mamykin, K. Tohji, B. Jeyadevan, K. Shinoda, T. Kudo, O. Terasaki, Z. Liu, R. V. Beloslu-dov, V. Sundararajan, Y. Kawazoe, *Nat. Mater.* 2004, **3**, 99 – 102.

38. J. Pedersen, S. Bjornholm, J. Borggreen, K. Hansen, T. P. Martin, H. D. Ra-smussen, *Nature.* 1991, **353**, 733–735.

39. Y. Wang, Y. H. Liu, Y. Zhang, P. J. Kowalski, H. W. Rohrs, W. E. Buhro, *Inorg. Chem.* 2013, **52**, 2933-2938.

40. M. A. Schreuder, J. R. McBride, A. D. Dukes III, J. A. Sammons, S. J. Ro-senthal, *J. Phys. Chem. C.* 2009, **113**, 8169-8176.

41. K. Knowles, D. B. Tice, E. A. McArthur, G. C. SolOMOn, E. A. Weiss, *J. Am. Chem. Soc.* 2009, **132**, 1041-1050.

42. K. Eichkorn, R. Ahlrichs, *Chem. Phys. Lett.* 1998, **288**, 235-242.

43. Deglmann, P.; Ahlrichs, R.; Tsereteli, K. *J. Chem. Phys.* 2002, **116**, 1585-1597.

44. K. Leung, K. B. Whaley, *J. Chem. Phys.* 1999, **110**, 11012-11022.

45. M. C. Troparevsky, J. R. Chelikowsky, *J. Chem. Phys.* 2001, **114**, 943-946.

46. M. C. Troparevsky, L. Kronik, J. R. Chelikowsky, *J. Chem. Phys.* 2003, **119**, 2284-2287.

47. A. Puzder, A. J. Williamson, F. Gygi, G. Galli, *Phys. Rev. Lett.* 2004, **92**, 217401.

48. P. Yang, S. Tretiak, A. Masunov, S. Ivanov, *J. Chem. Phys.* 2008, **129**, 074709.

49. C. J. Tian, P. Xiu, Y. Meng, W. Y. Zhao, Z. G. Wang, R. H. Zhou, *Chem. Eur. J.* 2012, **18**, 14305-14313.

50. Z. G. Wang, M. G. Yao, S. F. Pan, M. X. Jin, B. B. Liu, H. X. Zhang, *J. Phys. Chem. C.* 2007, **111**, 4473-4476.

51. X. Dai, C. Cheng, W. Zhang, M.S. Xin, P. Huai, R.Q. Zhang, Z.G. Wang, *Sci. Rep.* 2013, **3**, 1341.

52. A. E. Kuznetsov, D. Balamurugan, S. S. Skourtis, D. N. Beratan, *J. Phys. Chem. C.* 2012, **116**, 6817−6830.

53. A. D. Becke, *J. Chem. Phys.* 1993, **98**, 5648-5652.

54. C. Lee, W. Yang, R. G. Parr, *Phys. Rev. B*, 1988, **37**, 785-789.

55. B. Miehlich, A. Savin, H. Stoll, H. Preuss, *Chem. Phys. Lett.* 1989, **157**, 200-206.

56. R. Nadler, J. F. Sanz, *Theor. Chem. Acc.* 2013, **132**, 1-9.

57. P. Yang, S. Tretiak, S. Ivanov, *Journal of Cluster Science*, 2011, **22**, 405-431.

58. X. Q. Wang, Q. Zeng, J. Shi, G. Jiang, M. L. Yang, X. Y. Liu, G. Enrightb, K. Yu, *Chem. Phys. Lett.* 2013, **568**, 125–129.

59. B. P. Bloom, L. B. Zhao, Y. Wang, D. Waldeck, *J. Phys. Chem. B.* 2013, **117**, 22401-22411.

60. S. K. Muzakir, N. Alias, M. M. Yusoff, R. Jose, *Phys. Chem. Chem. Phys.* 2013, **15**, 16275-16285.

61. R. Ditchfield, W. J. Hehre, J. A. Pople, *J. Chem. Phys.* 1971, **54**, 724-728.

62. M. A. L. Marques, E. K. U. Gross, *Annu. Rev. Phys. Chem.* 2004, **55**, 427-455.

63. M. J. Frisch; G. W. Trucks; H. B. Schlegel; G. E. Scuseria; M. A. Robb; J. R. Cheeseman; G. Scalmani; V. Barone; B. Mennucci; G. A. Petersson; H. Nakatsuji; M. Caricato; X. Li; H. P. Hratchian; A. F. Izmaylov; J. Bloino; G. Zheng; J. L. Sonnenberg; M. Hada; M. Ehara; K. Toyota; R. Fukuda; J. Hasegawa; M. Ishida; T. Nakajima; Y. Honda; O. Kitao; H. Nakai; T. Vreven; J. A. Montgomery, Jr; J. E. Peralta; F. Ogliaro; M. Bearpark; J. J. Heyd; E. Brothers; K. N. Kudin; V. N. Staroverov; R. Kobayashi; J. Normand; K. Raghavachari; A. Rendell; J. C. Burant; S. S. Iyengar; J. Tomasi; M. Cossi; N. Rega; J. M. Millam; M. Klene; J. E. Knox; J. B. Cross; V. Bakken; C. Adamo; J. Jaramillo; R. Gomperts; R. E. Stratmann; O. Yazyev; A. J. Austin; R. Cammi; C. Pomelli; J. W. Ochterski; R. L. Martin; K. Morokuma; V. G. Zakrzewski; G. A. Voth; P. Salvador; J. J. Dannenberg; S. Dapprich; A. D. Daniels; O. Farkas; J. B. Foresman; J. V. Ortiz, Gaussian 09 Revision D.01, Wallingford CT, 2013.

64. C. Landes, C. Burda, M. A. El-Sayed, *Nano Lett.* 2001, **1**, 667-670.

65. G. Kalyuzhny, R. W. Murray, *J. Phys. Chem. B*, 2005, **109**, 7012-7021.

66. A. Peng, J. Wickham, A. P. Alivisatos, *J. Am. Chem. Soc.* 1998, **120**, 5343-5344.

67. A. H. Margaret, G. S. Philippe, *J. Phys. Chem.* 1996, **100**, 468-471.

68. R. A. Vogt, T. G. Gray, C. E. Crespo-Hernández, *J. Am. Chem. Soc.* 2012, **134**, 14808-14817.

69. H. Braunschweig, R. D. Dewhurst, K. Hammond, J. K. Mies, Radacki, A. Vargas, *Science.* 2012, **336**, 1420-1422.

70. M. Del Ben, R. W. A. Havenith, R. Broer, M. Stener, *J. Phys. Chem. C.* **2011**, *115*, 16782-16796.

71. K. A. Nguyen, P. N. Day, R. Pachter, *J. Phys. Chem. C.* 2010, **114**, 16197–16209.

TOC
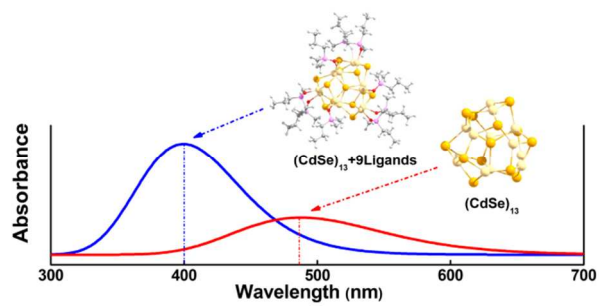
The absorption peak displays a clear blue-shift on the scale of 95 nm for quantum dots $(CdSe)_{13}$ passivated by $OPMe_2(CH_2)_nMe$ ligands in the ultraviolet-visible (UV-vis) spectra.